

Structural Properties and Gamma Rays Shielding of TeO₂-B₂O₃-PbO Glass System

M. S. Hafiz^{1*}, H.A. Othman², N. A. Kawady¹, I. Z. Hager², M. G. El-Feky¹, H. M. El-Samman²

¹Geochemical Exploration Department, Nuclear Materials Authority (NMA), P.O. Box 530, El-Maadi, Cairo, Egypt.

²Physics department, Faculty of Science, Menoufia University, Shibin El Kom, Egypt.

Received: 20 May .2020, Revised: 18 Jul .2020, Accepted: 14 Aug. 2020.

Published online: 1 Jan. 2021.

Abstract: Glass system of composition (80-x) TeO₂-20B₂O₃-xPbO (where x=2, 6, 10, 14 and 20 mol %) had been prepared by melt-quenching technique. Structure analysis were examined using X-ray diffraction (XRD), density, molar volume and fourier transform infrared (FTIR) spectroscopy measurements. Glass samples were irradiated by collimated gamma rays with different energies 0.662, 1.173 and 1.332 MeV emitted by ¹³⁷Cs and ⁶⁰Co radioactive point sources respectively. Radiation shielding factors such as mass attenuation coefficients (μ/ρ), half value layer (HVL), mean free path (mfp) and tenth value layer (TVL) have been determined experimentally using NaI(Tl) scintillation detector, and theoretically calculated using XCOM program. There was a slight variation between experimental and theoretical mass attenuation coefficient values. The shielding properties related to the structure of investigated tellurite glass samples. Noticed rising in shielding parameters values due to rise of lead oxide and boron oxide content in the tellurite glass sample structure.

Keywords: Tellurite glass, Mass attenuation coefficient; Mean free path, Half-value layer.

1 Introduction

Human beings are exposed to several types of ionizing radiation, like X-ray and gamma radiation; Gamma radiation has extreme penetration depth [1,2]. The researchers try to make various materials known as shielding materials [3-7]. The mainly important features of the chosen shielding materials are the cost of the materials used, the thermal, mechanical and optical properties of the materials used in applications like in the hospital X-ray rooms, radiation therapy rooms, airport security X-ray screens, for materials testing, nuclear facilities, laboratories, X-ray and radiation protection spectacles.

Polymers and Concretes are considered as traditional radiation shielding materials [8-12]. These materials have several disadvantages like cracks formation with long exposure to nuclear radiations, decrement in density and mechanical strength due to trapped water content and chemical damage etc. and that limit the applications of these materials. Glasses due to their high transparency in the visible zone are certainly better over opaque concretes for absorbing radiations like gamma-rays. Additionally,

glasses physical and chemical properties can be easily improved by changing the composition and choosing different preparing methods. Glasses fabrication cost is also cheap and easily can be prepared in large sizes with high

homogeneity [13-15]. It is well known that materials with

high atomic number elements and high density are appropriate to radiation shielding materials. [16,17]. Boric acid (B₂O₃) is one of the most common and excellent glass formers known to form glass at lower melting point with good transparency, thermal stability, high chemical durability, and thermal stability. Due to its higher bond strength, smaller cation size and heat of fusion, so the structural analysis of boron in borate glass is one of its advantages. Present of glass formers like TeO₂ and B₂O₃ increasing the forming range of the glass and allow to add more PbO which develop the shielding property [18,19]. Linear attenuation coefficient, mass attenuation coefficient, half value layer, Tenth value layer and mean free path are dependent on the structure of the radiation shielding samples [20-23]. The aim of the present work is preparing tellurite glass doped with high density elements like boron and lead, examining structure properties of the prepared glass systems. Examining the shielding properties and calculate gamma rays shielding parameters for the prepared glass system experimentally and theoretically.

2 Experimental Procedures

2.1 Glass Preparation

Tellurite glass system (Te20BPb) with composition (80-x)TeO₂-20B₂O₃-xPbO (where x = 2, 6, 10,14 and 20 mol%)

*Corresponding author e-mail: maisaeed366@gmail.com

were prepared by melt- quenching technique. The purity of the utilized chemicals is 99.9% for tellurium oxide (TeO_2 , Acros Organic), 99% for lead oxide (PbO , Sigma-Aldrich) and 99.5% for boric acid (H_3BO_3 , Sigma-Aldrich). The suitable ratios of raw materials were weighted and mixed in alumina crucible. The mixture was heated till melting point was obtained around 850 oC. Then the sample was steered and putted in the furnace for 20 min. The melted sample was put into a pre-heated stainless steel mold and then moved to an annealing furnace around at 380 °C for 1 h to remove internal stress. The gotten glass samples were polished for maximum smoothness. Glass samples have a circular shape with 2.2 cm diameter and thickness varies from 0.35 to 0.38 cm, also it has a transparent yellow appearance and good optical quality.

2.2 Structure Characterization

2.2.1 Fourier Transforms Infrared Spectroscopy

All glass samples were examined by a Thermo scientific nicolet10 FT-IR spectrophotometer (Thermo Fisher scientific, USA) over the wave number range of 4000–200 cm^{-1} at room temperature.

2.2.2 The Density and Molar Volume

The density was calculated for all glass samples using the Archimedean method with toluene as the immersion liquid at room temperature. The accuracy of the measurements was approximately $+0.01 \text{ g cm}^{-3}$.

The density of the samples is measured using Archimedean method as follows:

$$\rho_{\text{sample}} = \frac{\rho_{\text{liquid}} \times w_{\text{air}}}{w_{\text{air}} - w_{\text{liquid}}} \quad (1)$$

where w_{liquid} is weight of sample in toluene (immersion liquid) and w_{air} is weight of sample in air, and ρ_{liquid} is the density of toluene. The accuracy of density measurements is about $\pm 0.001 \text{ g cm}^{-3}$ [24].

The molar volume is also calculated using the relation;

$$V = \frac{MT}{\rho} \quad (2)$$

where MT is the total molecular weight and ρ is the density of glass sample [25].

2.2.3 X-ray Diffraction (XRD) Analysis

XRD analysis was done at room temperature for glass systems to confirm the amorphous nature of the glass samples using a Philips PW 3710/31 diffractometer. The instrument was calibrated using quartz and corundum calibration standards prior to use. Operated at 40 kV and 20 mA with $\text{Cu K}\alpha$ radiation ($\lambda=1.54\text{\AA}$) and a scan rate of 0.02 %. The powder samples were placed in quartz plate and scanned from 2θ equal to 4° to 80° .

2.3 Gamma Rays Shielding Parameters Measurements

2.3.1 NaI (Tl) Scintillation Detector

The gamma ray spectrometry system contains Bicon scintillation detector, NaI (Tl) crystal, 76x76 mm, hermetically sealed with a photomultiplier tube in aluminum housing. The detector is covered with its amplifier in a copper shield (0.6 cm thickness) against induced X-rays and a cylindrical lead chamber against the environmental radiations. The Accuspec NaI plus 2k on board ADC, Amp and HVPS with 2k chain memory which is attached to the PC computer board, at room temperature.

3 Results and Discussion

3.1 Structure Analysis of Glass

3.1.1 XRD Characterization

XRD patterns for the prepared glass samples were shown in figure 1. It is observed that no peaks were obtained; only a broad hump observed in X-ray diffraction pattern confirmed the amorphous nature of the glass samples.

Figure 1. X-Ray diffraction pattern for glass series Te20BPb

3.1.2 The glass Density and Molar Volume Characterization

The values of the density and molar volume of the examined glasses were collected in table1. The dependence of the glass density with composition of PbO content was shown in figure 2. The density increased as lead oxide contents increased. This attributed to the higher density and higher molecular weight of the doped lead oxide ($223.20 \text{ g mole}^{-1}$) in comparison with tellurium oxide ($159.60 \text{ g mole}^{-1}$).

Table 1: The values of TeO_2 (mol%), B_2O_3 (mol%), PbO (mol%), density, ρ , (gm.cm^{-3}) and molar volume of the glass system.

Sample Code	TeO_2	B_2O_3	PbO	P	V_m
Te20BPb-1	78	20	2	4.6	31.06
Te20BPb-2	74	20	6	4.9	29.67
Te20BPb-3	70	20	10	4.7	31.48
Te20BPb-4	66	20	14	5	30.13
Te20BPb-5	60	20	20	5.2	29.67

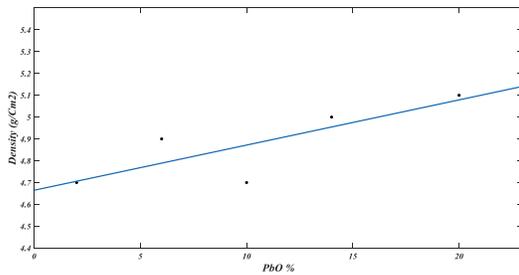


Fig. 2: Variation of density with lead oxide content for glass series Te20BPb.

Figure 3 presented the variation of molar volume of Te20BPb glass system with PbO content. The value of molar volume decreased from 31.06 cm³mol⁻¹ for the sample Te20BPb1 to 29.67 cm³mol⁻¹ for sample Te20BPb5. The molar volume was decreased with the increasing PbO content. This might be because of some changes in the glass structure. Decreasing in molar volume is attributed to the reduces in bond length or interatomic spacing between the atoms of glass network which causes compaction of the structure [26].

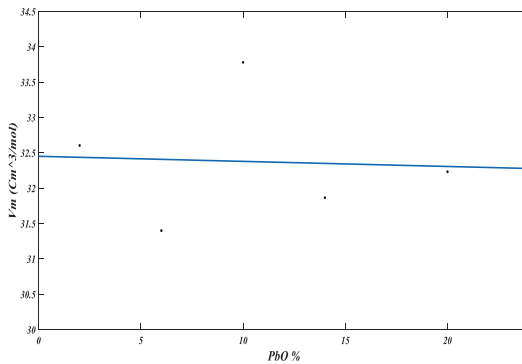


Fig.3: Variation of molar volume with PbO content for glass series Te20BPb.

3.1.3 FTIR Characterization

Figure 4 showed FTIR spectra for the glass samples. FTIR spectra decides the characteristic chemical bond exist between elements in the glass sample. Absorption peak in spectrum represents the frequencies of vibrations among the bonds of the atom or molecule. Tellurite oxide is characterized by two structural units; trigonal bipyramid (TeO₄) and trigonal pyramid (TeO₃). Pure TeO₂ is characterized by an infrared absorption at about 640 cm⁻¹ [27]. The band of absorption between 600-700 cm⁻¹ represents the stretching vibration of the Te-O in the trigonal bipyramid TeO₄ and trigonal pyramid TeO₃ [28]. The stretching vibration of TeO₃ group is between 650–700 cm⁻¹ while stretching vibration of TeO₄ which in between 600–650 cm⁻¹. The isolated absorption bands appear with maximum at around 1365 cm⁻¹ and at around 1235 cm⁻¹ due to the structural groups of the trigonally coordinated boron BO₃ (Figure 4). The absorption band that appears

with maximum at 668-684 cm⁻¹ due to stretching vibrations of the Te–O bond in the TeO₃ groups [29]. Increasing the lead oxide content from 2 to 20 mol % reasons small changes in their spectra (Figure 5), where the characteristic absorption bands for the BO₃ groups were slight shifted toward lower frequencies. This may be due to conversion of boron ions from three-coordination to four-coordination. PbO acts as a modifier of the structural network in the form of PbO₆ groups and promotes conversion of the BO₃ groups to BO₄ tetrahedral. By increasing the tellurium oxide content from 70 to 78 mol %, the position of the absorption band which at 671 cm⁻¹ shifted to 684 cm⁻¹ (Figure 6). Also, the shoulder one at around 1400 cm⁻¹ which attributed to stretching vibrations of B-O bond, begin to isolation and be stronger with the increasing of TeO₂ due to the formation of BO₄ tetrahedrons [30, 31].

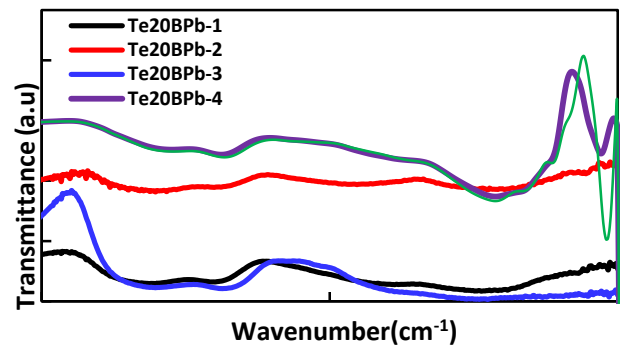


Fig. 4: FTIR spectra of the prepared glass series Te20BPb.

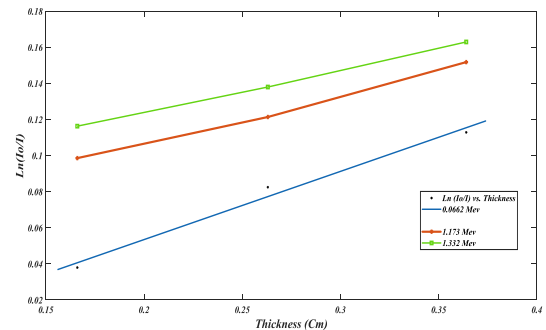


Fig. 5: Gamma transmission through glass sample Te20BPb-4 with different thicknesses at different energies.

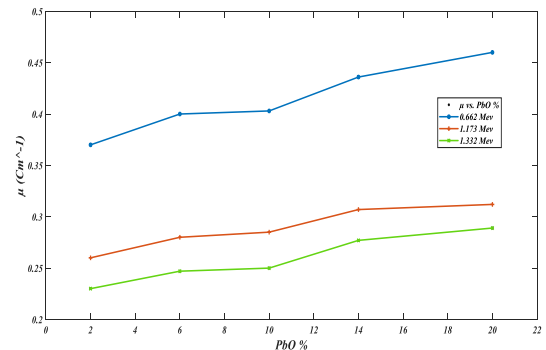


Fig. 6: Variation of linear attenuation coefficient with PbO content of glass series Te20BPb.

3.2 Shielding Properties

Shielding parameters of the prepared glass were calculated using narrow beam transmission technique and NaI (Ti) scintillation detector at 0.662, 1.173 and 1.332 MeV emitted from ^{137}Cs and ^{60}Co point sources respectively.

3.2.1 The Linear Attenuation Coefficient

Linear attenuation coefficient is a parameter that determined by using Beer- Lambert equation as follows;

$$\mu = \frac{\ln\left(\frac{I_0}{I}\right)}{x} \quad (3)$$

where I is photon energy counts with the thickness of shielding material, I_0 is photon energy counts in absence of glass sample, x is the thickness of the shielding material and μ is the linear attenuation coefficient [32]. It was evaluated from linear graph of $\ln(I_0/I)$ with different thicknesses of glass sample X where the slope equal to linear attenuation coefficient value (Figure 7). Table 2 showed the calculated linear attenuation coefficient values for both series of the glass samples which has different content of lead oxide and boron oxide at different energies. It clear from figure 8 that linear attenuation coefficient increased with the increasing of lead oxide content at different energies. Linear attenuation increased by increasing density and atomic number of lead.

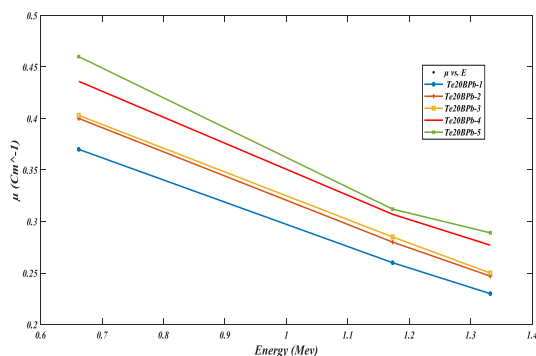


Fig. 7: Variation of linear attenuation coefficient with energy for glass series Te20BPb.

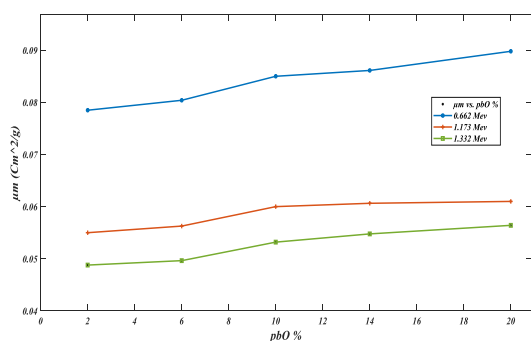


Fig. 8: Variation of mass attenuation coefficient with PbO content for glass series Te20BPb at different energies.

Table 2: Linear attenuation coefficients (cm^{-1}) for both series of the prepared glass series (Te20BPb) at different energies (MeV).

Sample Code	Linear attenuation coefficients (cm^{-1})		
	0.662 MeV	1.173 MeV	1.332 MeV
Te20BPb-1	0.37	0.26	.23
Te20BPb-2	0.40	0.28	0.247
Te20BPb-3	0.403	0.285	0.25
Te20BPb-4	0.436	0.307	0.277
Te20BPb-5	0.46	0.312	0.289

Linear attenuation coefficient varies with energy. Figure 9 presented the decreasing of linear attenuation coefficient with the increasing of energy.

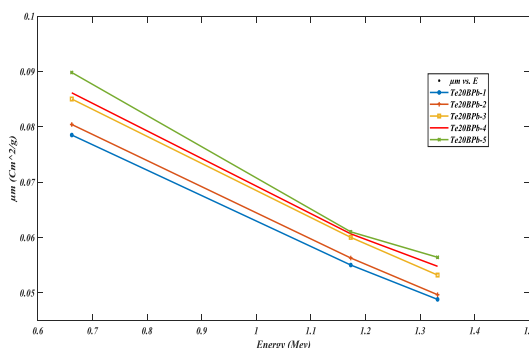


Fig.9: Variation of mass attenuation coefficient with energy for glass series Te20BPb.

3.2.2 The Mass Attenuation Coefficient

The mass attenuation can be calculated from the relation [33],

$$\mu_m = \ln\left(\frac{I_0}{I}\right) / \rho x \quad (4)$$

where ρ is the density of shielding material. Mass attenuation coefficient can be determined experimentally by any type of gamma rays detector moreover it can be determined theoretically by NIST XCOM software [34] using equation 5.

$$\mu_m = \sum_i w_i \mu_i \quad (5)$$

where μ_i and w_i are percentage by mass attenuation coefficient and weight of the i th element of the mixture sample. Mass attenuation coefficient values with the obtained values of density were utilized for mass attenuation coefficient (Equation 4) determination. Figure 8 presented the relation between mass attenuation coefficient and lead oxide concentration of glass system (Te20BPb). It is observed from figure 10 that the mass attenuation coefficient increases with the increasing of lead oxide content for all energies. The mass attenuation coefficient showed the same behavior as linear attenuation coefficient (higher density and higher atomic number of lead oxide). It increased from $0.0784 \text{ cm}^2 \text{ g}^{-1}$ of sample

Te20BPb-1 to 0.08979 cm²/g for sample Te20BPb-5 content for glass samples of series Te20BPb at 0.662 MeV. This declared that the higher mass attenuation coefficient in the glass system is at 20 mol% lead oxide content which has composition 60TeO₂- 20B₂O₃-20PbO. This glass sample has the higher doped concentration of lead oxide than other samples. In general, the increasing ratio of PbO in tellurite glass systems, increase mass attenuation coefficient.

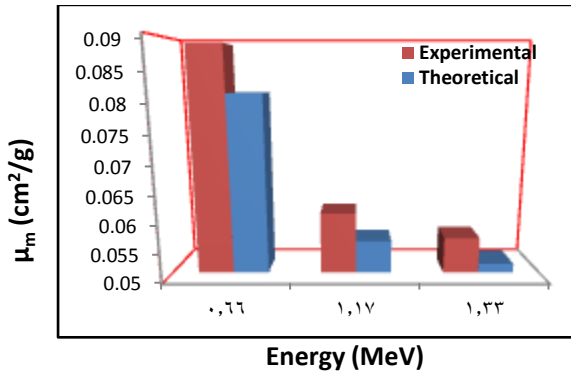


Fig.10: Comparison between experimental and theoretical mass attenuation coefficients for the prepared 20% PbO content glass sample of the glass series at different energies.

Figure 11 showed the relation between mass attenuation coefficient and energy. When energy increases from 0.662 MeV to 1.332 MeV, mass attenuation coefficient decreases as less interaction between gamma rays and glass samples in other words transmitted and less absorbed gamma rays increases. The interaction between gamma rays and glass samples along with energy variation was as follows: pair production at high energy above 1.022 MeV, Compton scattering dominates at intermediate energy range and photoelectric effect dominates at low energy range.

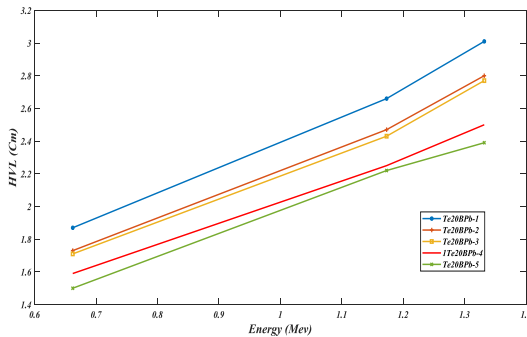


Fig. 11: Variation of HVL (cm) with energy (MeV) for glass series Te20BPb.

To approve the accuracy of the calculated experimental mass attenuation coefficients, it has been calculated theoretically using XCOM program which it can calculate mass attenuation coefficients for an element, composite and mixture of elements ($Z \leq 100$) within 1 Kev-100Gev photon energy range. It uses equation 5 for mass attenuation determination [36].

Table 3 and Figure 12 showed a comparison between experimental μ/ρ and theoretical values. The deviation (Dev %) between these two techniques can be determined using the following equation;

$$\text{Dev \%} = \frac{\mu_m(\text{tho}) - \mu_m(\text{exp})}{\mu_m(\text{tho})} \times 100 \quad (9)$$

The deviation was observed to be less than 10 %. This shows that there is a small difference between experimental and theoretical mass attenuation coefficients for the prepared borotellurite glass doped lead oxide at different energies [35]. The difference between experimental and theoretical mass attenuation coefficients are attributed to the difference between employed techniques database and utilized extended nuclear cross section libraries [36]. Glass sample Te20BPb-5 has the highest mass attenuation coefficient value which equal to 0.0897cm²g⁻¹. If we compare this value with mass attenuation coefficient value of lead which equal to 0.1101 cm²g⁻¹ [37, 38], it can be conclude that it represents 81.4 % from lead value. The result approves the efficiency of borotellurite glass doped lead oxide for gamma rays shielding.

3.2.3 The Half Value Layer and the Tenth Value Layer

The choice of shielding material for application purpose depend on Half value layer (HVL) shielding parameter which defined as the thickness from shielding material that reduces the initial intensity of gamma rays to its half value as equation 6. Tenth value layer is another shielding parameter that is similar to HVL but it represents the thickness from shielding material that reduces intensity of gamma rays to one tenth of its initial intensity according to equation 7 [39, 40].

3.2.4 The Mean Free Path

Mean free path (mfp) is the average distance between two interactions of gamma rays and shielding material and can be illustrated mathematically in equation 8 [41, 42].

$$\text{mfp} = \frac{1}{\mu} \quad (8)$$

where μ is the calculated linear attenuation coefficient. The HVL, TVL and mfp should be low as possible. The resulting values are tabulated in table 4. The relation between HVL, TVL and mfp with the energy (MeV) are shown in figures 11, 12 and 13 respectively. It is noticed from these figures that the addition of PbO significantly reduces HVL, TVL and mfp. This because of PbO has high density and high atomic number and then increases the density of the glass samples. HVL decreased from 1.87, 2.66 and 3.01 to 1.5, 2.22 and 2.39 at 0.662 MeV for glass samples of series Te20BPb. TVL and mfp has the same behavior as HVL Te20BPb-5 glass sample of composition (60TeO₂.20B₂O₃.20PbO) is the best sample as it has the lowest HVL, TVL and mfp than other samples in addition to it has the highest mass attenuation coefficient because it has the highest PbO doping, highest B₂O₃.

Table 3: Experimental and theoretical mass attenuation coefficients for the prepared glass samples glass series (Te20BPb) at different energies and the corresponding deviation.

Energy (MeV)		0.662			1.173			1.332		
		μ_m (ex)	μ_m (th)	Dev . %	μ_m (ex)	μ_m (th)	Dev %	μ_m (ex)	μ_m (th)	Dev.%
	Te20BPb-1	0.07	0.07	-3.4	0.05	0.05	-2.9	0.04	0.05	3.3
	Te20BPb-2	0.08	0.07	-4.1	0.05	0.05	-3.4	0.04	0.05	2.1
	Te20BPb-3	0.08	0.07	-9.3	0.06	0.05	-9.6	0.05	0.05	-4.3
	Te20BPb-4	0.08	0.07	-8	0.06	0.05	-9	0.05	0.05	-6.8
	Te20BPb-5	0.08	0.08	-9.9	0.06	0.05	-9.1	0.05	0.05	-9.3

Table 4: HVL, TVL and mfp (cm) values for glass samples of glass series (Te20BPb) at different energies.

energy (MeV)	0.662			1.173			1.332		
	HVL (cm)	TVL (cm)	mfp (cm)	HVL (cm)	TVL (cm)	mfp (cm)	HVL (cm)	TVL (cm)	mfp (cm)
Te20BPb-1	1.8	6.2	2.7	2.6	8.8	3.8	3.0	10.0	4.3
Te20BPb-2	1.7	5.7	2.5	2.4	8.2	3.5	2.8	9.3	4
Te20BPb-3	1.7	5.7	2.4	2.4	8.07	3.5	2.7	9.2	4
Te20BPb-4	1.6	5.2	2.3	2.2	7.50	3.2	2.5	8.3	3.6
Te20BPb-5	1.5	5.0	2.1	2.2	7.3	3.2	2.3	7.9	3.4

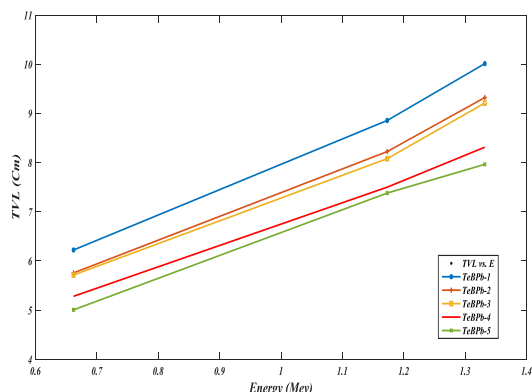


Fig. 12: Variation of TVL (cm) with energy (MeV) for glass series Te20BPb.

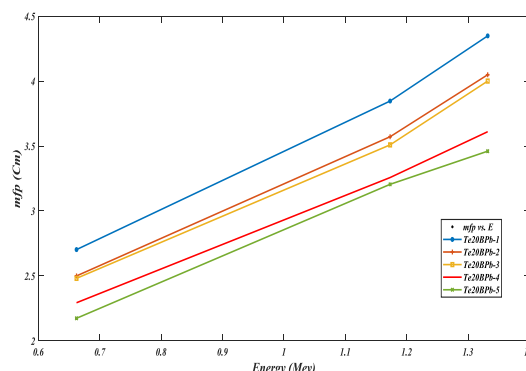


Fig.13: Variation of mfp (cm) with energy (MeV) for glass series Te20BPb

4 Conclusions

The prepared borotellurite glasses doped with different lead content are characterized by a high density ranging from 4.6 g cm⁻³ to 5.2 g cm⁻³. The molar volume values range from 31.06 cm³ mol⁻¹ to 29.67 cm³ mol⁻¹. X-rays diffraction pattern verify the amorphous nature of the glass samples. Shielding parameters increase due to the increase of lead oxide and tellurium oxide. All glass samples showed high value of mass attenuation coefficient and less HVL, TVL and mfp but the highest mass attenuation coefficient value is the glass sample with composition 60TeO₂.20B₂O₃.20PbO also it has the lowest HVL, TVL and mfp. There is a small difference between experimental and theoretical mass attenuation coefficients. The deviation between experimental and theoretical mass attenuation coefficients is less than 10%. The comparison between the best sample in mass attenuation coefficient value (0.0897 cm² g⁻¹) and lead value (0.1101 cm²g⁻¹) illustrate that it represent 81.4 % from lead value. The result clarifies that borotellurite glass samples doped with lead are very good gamma rays shielding materials which can be used in many applications.

References

- [1] H. Gökce, C.Yalcinkaya, M. Tuyan, Optimization of reactive powder concrete by means of barite aggregate for both neutrons and gamma rays, *Journal of Construction and Building Materials.*, **189**, 470–477 (2018).
- [2] V. Beir, Health effects of exposure to low levels of ionizing radiation, *Journal of The National Academy of Sciences Engineering Medicine*, Fifth Printing., **436** (1997).
- [3] S. Ruengsri, S. Insiripong, N. Sangwaranatee, J. Kaewkhao, Development of barium borosilicate glasses for radiation shielding materials using rice husk ash as a silica source, *Journal of Progress in Nuclear Energy.*, **83**, 99–104 (2015).
- [4] S. Obaid, M. Sayyed, D. Gaikwad, P. Pawar, Attenuation coefficients and exposure buildup factor of some rocks for gamma ray shielding applications, *Journal of Radiation Physics and Chemistry.*, **148**, 86-94 (2018).
- [5] M. Singh, A. Tondon, B. Sandhu, B. Singh, Energy dependence of radiation interaction parameters of some organic compounds, *Journal of Radiation Physics and Chemistry.*, **145**, 80-88 (2018).
- [6] H. Manjunatha, L. Seenappa, B. Chandrika, C. Hanumantharayappa, A study of photon interaction parameters in barium compounds, *Journal of Annals of Nuclear Energy.*, **109**, 1-726 (2017).
- [7] S. Obaid, D. Gaikwad, P. Pawar, Determination of gamma ray shielding parameters of rocks and concrete, *Journal of Radiation Physics and Chemistry.*, **144**, 356–360 (2018).
- [8] W. Guo-hui, Man-liHe., Chai, Fan-chao, Feng, J.-dong, D. Yao-dong, Enhancement of flame retardancy and radiation shielding properties of ethylene vinyl acetate based radiation shielding composites by EB irradiation, *Journal of Progress in Nuclear Energy.*, **112**, 225–232(2019).
- [9] D. Yılmaz, B. Aktaş, Cahk, O. Aytar, Boronizing effect on the radiation shielding properties of Hardox 450 and Hardox HiTuf steels, *Journal of Radiation Physics and Chemistry.*, **161**, 55–59(2019).
- [10] M. Roslan , M. Ismail, A. Kueh , M. Zin, High-density concrete: exploring Ferro boron effects in neutron and gamma radiation shielding, *Journal of Construction and Building Materials.*, **215**, 718–725(2019).
- [11] E. Waly, M. Bourham, Comparative study of different concrete composition as gamma-ray shielding materials, *Journal of Annals of Nuclear Energy.*, **85**, 306–310(2015).
- [12] T. Shams, M. Eftekhar, A. Shirani, Investigation of gamma radiation attenuation in heavy concrete shields containing hematite and barite aggregates in multilayered and mixed forms, *Journal of Construction and Building Materials.*, **182**, 35–42 (2018).
- [13] P. Limkitjaroenporn, J. Kaewkhao, P. Limsuwan , W. Chewpraditkul , Physical, optical, structural and gamma-ray shielding properties of lead sodium borate glasses, *Journal of Physics and Chemistry of Solids.*, **72**, 245–251(2011).
- [14] M. Sayyed, S. Qashou , Z. Khattari , Radiation shielding competence of newly developed TeO₂-WO₃glasses, *Journal of Alloys and Compounds.*, **696**, 632–638(2017).
- [15] M. Sayyed, K. Kaky, D. Gaikwad, O. Agar, U. Gawai, S. Baki, Physical, structural, optical and gamma radiation shielding properties of borate glasses containing heavy metals (Bi₂O₃/MoO₃), *Journal of Non-Crystalline Solids.*, **507**, 30-37(2015).
- [16] N. Ovcharenko, T. Smirnova, High refractive index and magneto–optical glasses in the systems TeO₂–WO₃–Bi₂O₃ and TeO₂–WO₃–PbO, *Journal of Non-Crystalline Solids.*, **291**, 121–126(2001).
- [17] D. Lezal, J. Pedlikova, P. Kostka, J. Bludska, M. Poulain, J. Zavadil, Heavy metal oxide glasses: preparation and physical properties, *Journal of Non-Crystalline Solids .*, **284**, 288- 295 (2001).
- [18] Y. Dimitriev, B. Samuneva, Y. Ivanova, E. Gattef, Y. Michailova, A. Staneva, Glass formation and crystallization in the Bi-Sr-Ca-Cu-O system, *Journal of Superconductor Science and Technology.*, **3**, 606-610 (1990).
- [19] R. El-Mallawany, M. Sayyed, M. Dong, Y. Rammah, Simulation of Radiation Shielding Properties of Glasses Contain PbO, *Journal of Radiation Physics and Chemistry.*, **151**, 239-252 (2018).
- [20] E. Şakar, M. Buyukyıldız, B. Alım, B. Şakar, M. Kurudirek, Leaded brass alloys for gamma-ray shielding applications, *Journal of Radiation Physics*

- and Chemistry., **159**, 64–69(2019).
- [21] A. El-Taher, H.M. Mahmoud and Adel G.E. Abbady Comparative Study of Attenuation and Scattering of Gamma –Ray through Two Intermediate Rocks. *Indian Journal of Pure & Applied Physics*, **45** (2007).
- [22] K. Mann, Investigation of gamma-ray shielding by double layered enclosures, *Journal of Radiation Physics and Chemistry.*, **159**, 207–221(2019).
- [23] O. Agar, M. Sayyed, F. Akman, H. Tekin, M. Kacal, An extensive investigation on gamma ray shielding features of Pd/Ag based alloys, *Journal of Nuclear Engineering and Technology.*, (**51**) 853–859 (2019).
- [24] W. Hughes Stephen, Measuring liquid density using Archimedes' principle, *Journal of Physics Education.*, **41(5)**, (2006).
- [25] RM El-Sharkawy, KS Shaaban, R Elsaman, EA Allam, Atef El-Taher, Investigation of mechanical and radiation shielding characteristics of novel glass systems with the composition $x\text{NiO}-20\text{ZnO}-60\text{B}_2\text{O}_3-(20-x)\text{CdO}$ based on nanometal oxides *Journal of Non-Crystalline Solids.*, **528**, 119754(2020) .
- [26] A. Mardhiah, W. Hanif , K. Azman , N. Yahya, The Physical Properties Of Lead Borate ($\text{PbO}-\text{B}_2\text{O}_3$)Glass. *KONAKA* (2015).
- [27] P. Gayathri Pavani, K. Sadhana, V. Chandra Mouli, Optical, physical and structural studies of boro-zinc tellurite glasses. *Physica B: Condensed Matter .*, **406**, 1242-1247 (2011).
- [28] G. Rachkovskaya, and G. Zakharevich, IR spectra of tellurium germanate glasses and their structure. *Journal of Applied Spectroscopy.*, **74**, 86-89(2007).
- [29] G. Rachkovskaya and G. Zakharevich, IR spectra of tellurium germanate glasses and their structure. *Journal of Applied Spectroscopy.*, **74**, 86-89(2007).
- [30] N. Pavlushkin and A. Zhuravlev, Low-Melting Glasses [in Russian], *Energiya, Moscow*.p 144(1970).
- [31] Y. Zhou, Y. Yang, F. Huang, J. Ren, S. Yuan, and G. Chen, Characterization of new tellurite glasses and crystalline phases in the $\text{TeO}_2\text{-PbO-Bi}_2\text{O}_3\text{-B}_2\text{O}_3$ system, *Journal of Non-Crystalline Solids.*, **386**, 90-94 (2014).
- [32] S. El-Fiki , S. El Kameesy, D. Nashar, , Abou- Leila, M.A. El-Mansy, M.Ahmed, Influence of bismuth contents on mechanical and gamma ray attenuation properties of silicone rubber composite, *International Journal of Advanced Researc.*, **3**, 1035–1039(2015).
- [33] S. Gounhalli, A. Shantappa, S. Hanagodimath , Studies on mass attenuation coefficient, effective atomic numbers and electron densities of some narcotic drugs in the energy range 1KeV–100GeV, *IOSR Journal of Applied Physics.*, **2**, 40–48(2012).
- [34] M. Berger, J. Hubbell, XCOM: Photon cross sections data base, Web Version, 1.2. National Institute of Standards and Technology, Gaithersburg, MD20899, USA. (Originally published as NBSIR., 87-3597
- “XCOM: Photon Cross Sections on a Personal Computer”), .(1999).
- [35] A. Un, Y. Sahin, Determination of mass attenuation coefficients, effective atomic and electron numbers, mean free paths and kermas for PbO, barite and some boron ores, *journal of Nuclear Instruments and Methods in Physics Research Section B: Beam Interactions with Materials and Atoms.*, **269**, 1506-1511 (2011).
- [36] R. Bagheri, S. Shirmardi, A. Ruhollah, Study on Gamma-ray Shielding Characteristics of Lead Oxide, Barite and Boron Ores using MCNP-4C Monte Carlo code and Experimental data, *Journal of Testing and Evaluation.*, **45**, 2259-2266 (2016).
- [37] I. Hager, Y. Rammah, H. Othman, E. Ibrahim, S. Hassan, F. Sallam, Nano-structured natural bentonite clay coated by polyvinyl alcohol polymer for gamma rays attenuation, *Journal of Theoretical and Applied Physics.*, **13**, 141–153 (2019).
- [38] F. Sallam, I. Hager, Y. Rammah, H. Othman, S. Hassan, E. M Ibrahim. and Z. Ahmed, Evaluation of Gamma Rays Shielding Competence for Bentonite Clay /PVA Polymer Matrix Using MCNPX Code , *Arab Journal of Nuclear Sciences and Applications.*, **53**, 177-188 (2020).
- [39] Y. Rammah, M. Sayyed, A. Abohaswa, H. Tekin, FTIR, electronic polarizability and shielding parameters of B_2O_3 glasses doped with SnO_2 , *Journal of Applied Physics A Materials Science & Processing .*, **124**, 1-9 (2018).
- [40] M. Sayyed, Half value layer, mean free path and exposure buildup factor for tellurite glasses with different oxide compositions, *Journal of Alloys and Compounds.*, **69**, 3191–3197(2017).
- [41] A. Ali, Y. Rammah , M. Shaaban, The influence of TiO_2 on structural, physical and optical properties of $\text{B}_2\text{O}_3\text{-TeO}_2\text{-Na}_2\text{O-CaO}$ glasses, *Journal of Non-Crystalline Solids.*, **514**52–59(2019).
- [42] R. Bagheri, A. Moghaddam, H. Yousefnia, Gamma ray shielding study of barium-bismuth-borosilicate glasses as transparent shielding materials using MCNP-4C Code, XCOM program, and available experimental data. *Nucl. Eng. Technol.*, **49**, 216–223(2017).

